CHAPTER IV
RESULTS AND DISCUSSION

4.1 Lithium Ferrite Characterization

4.1.1 Scanning Electron Microscopy (SEM)

Scanning Electron Microscopy (SEM) analysis was applied to determine the average grain size of the synthesized $LiFe_5O_8$ compound. Prior to examination, the sample was homogeneously ground in a mortar for half an hour. Since $LiFe_5O_8$ is not very conductive, a gold sputter coating was applied in order to improve the SEM image. This gold sputter coating makes the sample more conductive by adsorbing into the sample at a micrometer or so of thickness. As a result, the electron beam has better contact on the sample, hence giving a shaper image. Energy Dispersive X-ray analysis (EDX) was not performed because lithium is not able to be characterized by this technique. The $LiFe_5O_8$ was found to be fairly uniform. Figure 4.1 shows an average grain size of 100 micrometres for the $LiFe_5O_8$ powder after the gold sputter coating was applied.

Figure 4.1 SEM image of $LiFe_5O_8$ with 100x magnification.

4.1.2 X-Ray Diffraction (XRD)

4.1.2.1 $LiFe_5O_8$ Powder

The synthesized lithium ferrite was also investigated by X-Ray Diffraction (XRD) to determine its composition and phase. The XRD results show that most of the peaks belong to $LiFe_5O_8$ in the cubic phase as shown in Figure 4.2. However, there is an intermediate compound with a similar phase to $LiFe_5O_8$ present in the sample which is identified as $LiFeO_2$. $LiFeO_2$ is probably unreacted from the starting material.

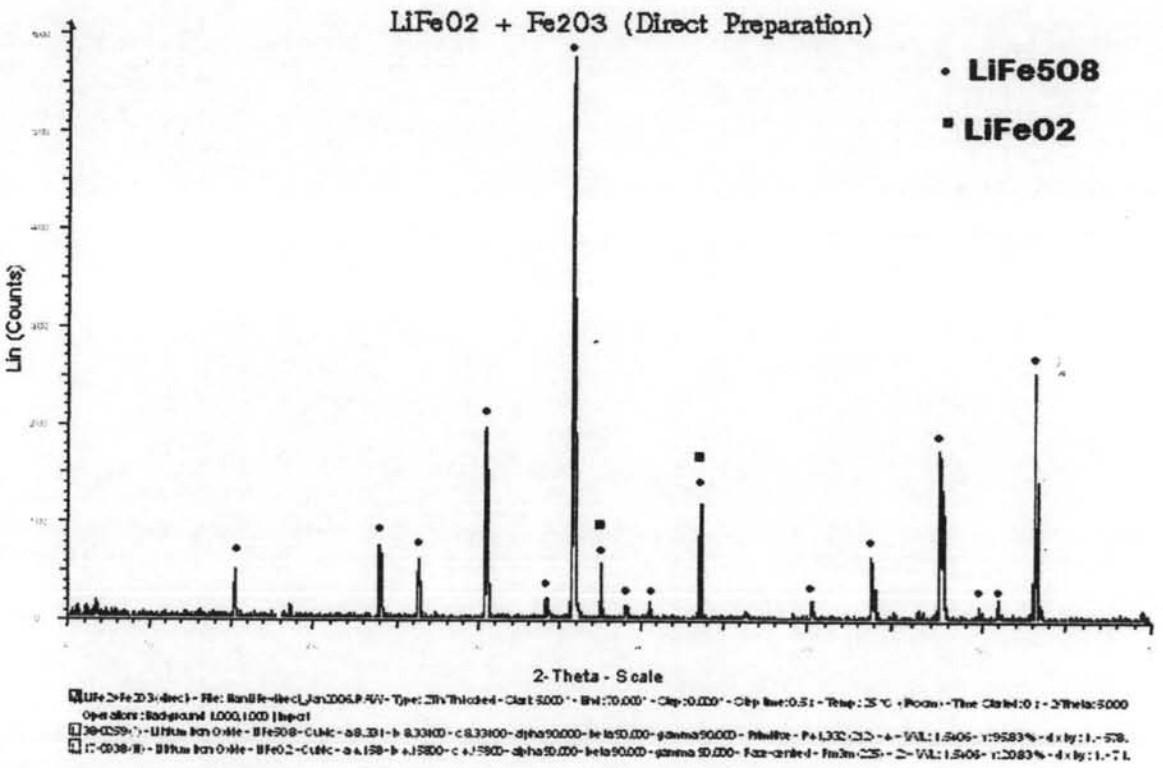

Figure 4.2 XRD pattern for $LiFe_5O_8$ prepared from $LiFeO_2$ and Fe_2O_3.

The crystal structure of γ-Fe_2O_3 and $LiFe_5O_8$ are similar since both have a cubic structure but are different in the crystal axis's (a,b and c). When $LiFe_5O_8$ was first characterized by XRD, without any element restriction in XRD, only the $LiFe_5O_8$ pattern was matched to all the peaks and maghemite (γ-Fe_2O_3) was not shown. When the maghemite pattern was added to match the peak sample, the peak

positions were similar but of lesser intensity, therefore it is confirmed that $LiFe_5O_8$ was formed not γ-Fe_2O_3.

4.1.2.2 $LiFe_5O_8$ Solid on Platinum Wire

XRD was used to ensure that $LiBO_2$ did not react chemically with $LiFe_5O_8$ to alter its phase and structure during the melting process in the furnace and subsequent solidification. Figures 4.3, 4.4 and 4.5 show the XRD patterns of the $LiFe_5O_8$ phase after it has been through the solidification process with different $LiBO_2$ ratios (1:2, 1:1 and 2:1) to create the liquid melt at high temperature. In order to analyze the solidified phase, some of the oxide was scraped off the platinum wire and ground to obtain a large enough sample for XRD measurement. When comparing Figure 4.3 to 4.5, it can be concluded that $LiFe_5O_8$ does not change its crystal structure or its phase no matter which ratio was applied. This flux agent is said to only lower the fusion temperature and the viscosity of the sample without creating any interelement effects. The noise between $10<2\theta<15$ in Figure 4.3 is due to the plexi glass sample holder because an insufficient amount of the powder was in the holder and the grain size of the sample was so small that the X-ray was detecting the powder as well as the plexi glass sample holder.

Even though the XRD patterns of the different $LiBO_2$ ratios show exactly the same compound structure, molten $LiFe_5O_8$ was formed the least with a low ratio (1:2 $LiBO_2$:$LiFe_5O_8$) and was not a homogeneous mixture. Therefore, it is not advised to use this ratio because it forms an inadequate amount of molten $LiFe_5O_8$ to be coated onto a platinum wire.

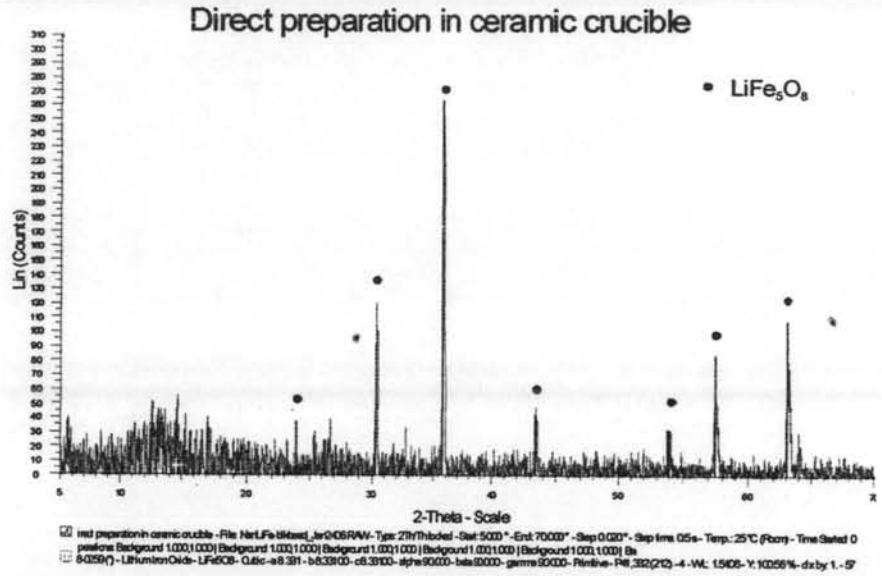

Figure 4.3 XRD pattern showing the $LiFe_5O_8$ phase after it has been through the coating process with $LiBO_2$ with a high ratio (2:1) at 1100°C.

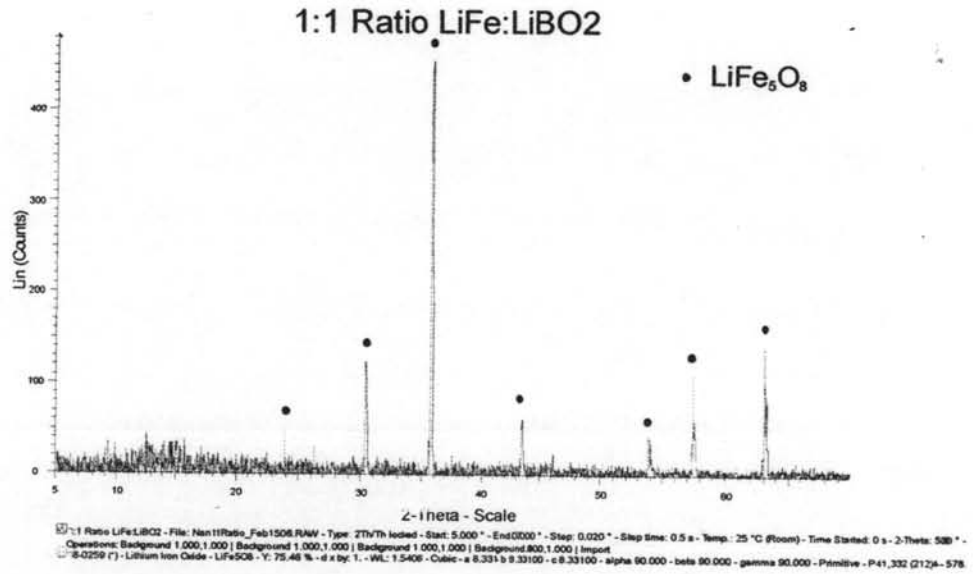

Figure 4.4 XRD pattern showing the $LiFe_5O_8$ phase after it has been through the coating process with $LiBO_2$ with an equimolar ratio (1:1) at 1100°C.

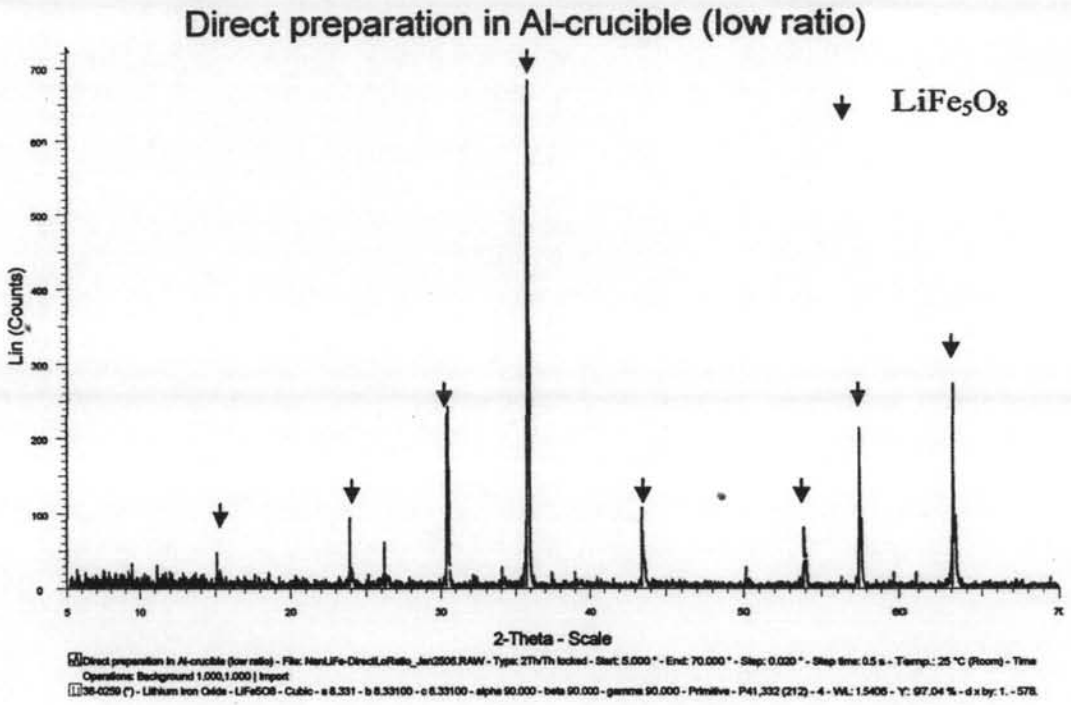

Figure 4.5 XRD peaks showing the $LiFe_5O_8$ phase after it has been through the molten process with $LiBO_2$ with a low ratio (1:2) at 1100°C.

4.1.3 Laser Raman Spectroscopy

This technique was used as a second validation tool for the $LiFe_5O_8$ phase and to examine the surface products formed on the compound following a polarization experiment. A pure $LiFe_5O_8$ powder was first used to establish its Raman spectras the same sample from the XRD (Figure 4.6).

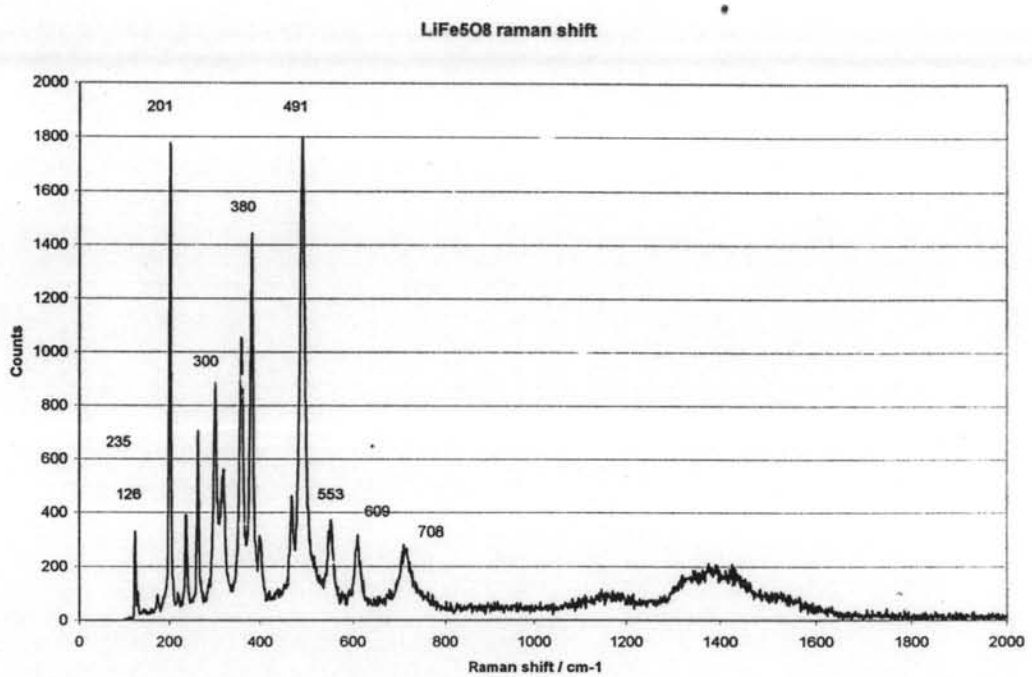

Figure 4.6 Raman shift pattern for a pure $LiFe_5O_8$.

In order to analyze the reaction products, the reaction was accelerated in the forward direction by using an electrochemical polarization technique. This polarization technique was applied in order to force the reaction to the right, yielding the reaction products which are believed to be either hematite, maghemite (γ-Fe_2O_3) and magnetite (Fe_3O_4). After the polarization experiments, the $LiFe_5O_8$ was immersed in concentrated HCl for several hours to increase the reaction rate so that the products of its decomposition could be analyzed. Following dissolution in the HCl, the acid turned bright yellow indicating the presence of ferric (Fe^{3+}) ion and there was a grey-black particulate left on the bottom of the beaker. The particulate

was filtered under vacuum and dried in the furnace at 50°C for an hour and then analyzed with the Raman spectrometer.

Figure 4.7 shows the Raman spectra of the particulate after the dissolution process. It is expected to be either maghemite or hematite due to visual information (red brownish compound on the $LiFe_5O_8$ surface) during the potential measurement. The numbers indicate peak positions of the $LiFe_5O_8$ spectra.

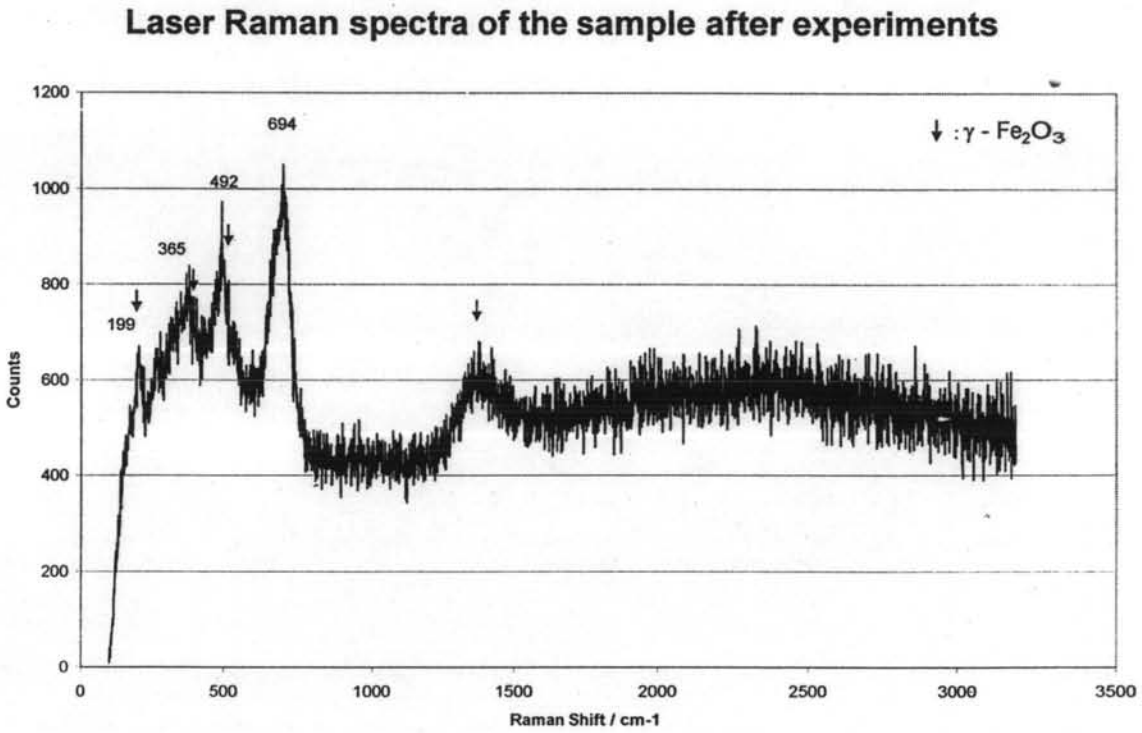

Figure 4.7 Raman shift pattern for unknown compound from $LiFe_5O_8$ after several polarization experiments.

When compared with the Raman shift of maghemite to $LiFe_5O_8$ spectra, all the peaks were shifted slightly to the left with some change in dominant peaks. This shift may be due to poor crystallinity of maghemite being formed during the polarization experiment. From Figure 4.6, the dominant peaks are at 491 cm^{-1} and 201 cm^{-1} whereas in Figure 4.7, the dominant peaks is at 694 cm-1 and 492 cm^{-1}. Since the dominant peaks have changed, it is likely that $LiFe_5O_8$ has undergone a transformation during polarization.

The arrows in Figure 4.7 indicate the maghemite spectra as reported from the literature shown in Table 4.1. All the peaks are slightly shifted to the left; however, it is believed that it is a maghemite compound.

Table 4.1 γ-Fe_2O_3 Raman spectra from literature. The strongest peak in each compound is underlined (Thierry *et al.*, 1988)

Table I. Wavelength shift (cm^{-1}) of major Raman peaks from iron and chromium containing reference compounds; the strongest peak in each compound is underlined.											
α-Fe_2O_3 single crystal (14)	α-Fe_2O_3 poly-crystal (present work)	γ-Fe_2O_3 powder (present work)	Fe_3O_4 theoretical (15)	Fe_3O_4 poly-crystal (present work)	α-FeOOH precipitate (16)	α-FeOOH powder (present work)	α-FeOOH mineralogical sample (present work)	γ-FeOOH precipitate (16)	γ-FeOOH powder (present work)	α-Cr_2O_3 single crystal (14)	α-Cr_2O_3 powder (present work)
612	613	740-650	676	670	550	560	557		660	609	602
500	500		550	550	474	470	489	380	380	551	541
413	412	505	420		397	385	397	252	252	530	
298	299	380	320		298	300	308			397	
293		350	298			250				351	342
245	247	263								303	306
226	225	193									
The peak may be broadened by traces of Fe_3O_4											

4.2 Determination of $LiFe_5O_8$ Potential

The open-circuit potential (OCP) of the $LiFe_5O_8$ coated platinum wire was measured under different Li concentrations from Li_2CO_3 solution to establish its Nernstian behavior. Figure 4.8 shows the potential under these various lithium concentrations (10^{-5}, 10^{-4} and 10^{-3} M). As expected, the higher lithium concentration of test solution established lower lithium ferrite potentials. All the potentials were measured against a standard calomel electrode (SCE), therefore the potential is indicated as V_{SCE} unless stated otherwise.

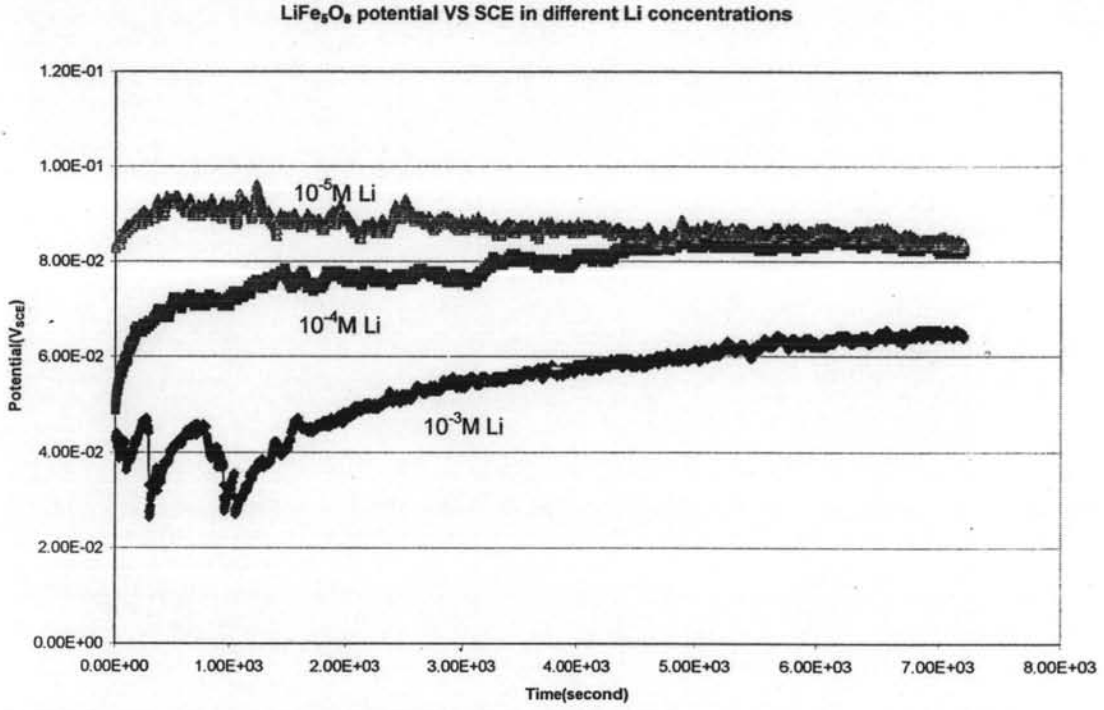

Figure 4.8 $LiFe_5O_8$ potential measurement against SCE in different Li concentrations.

The potential measurements were also conducted as a function of the pH of the testing solution. The pH was changed by adding small amounts of 0.1M HCl until the desired value was obtained. It is assumed that the small amount of HCl added to the solution did not significantly change the lithium concentration in the

solution. After HCl was added into the testing solution, the potential was again measured against SCE.

Figure 4.9 and 4.10 show the plots between potential of $LiFe_5O_8$ and pH at 10^{-3}M Li_2CO_3 and 10^{-3}M LiOH respectively. The potential decreases as pH increases as expected through the Nernst equation. Different ratio of $LiFe_5O_8$ electrodes (high ratio and equimolar ratio) were compared in 10^{-3}M LiOH solution to validate their characteristics at room temperature.

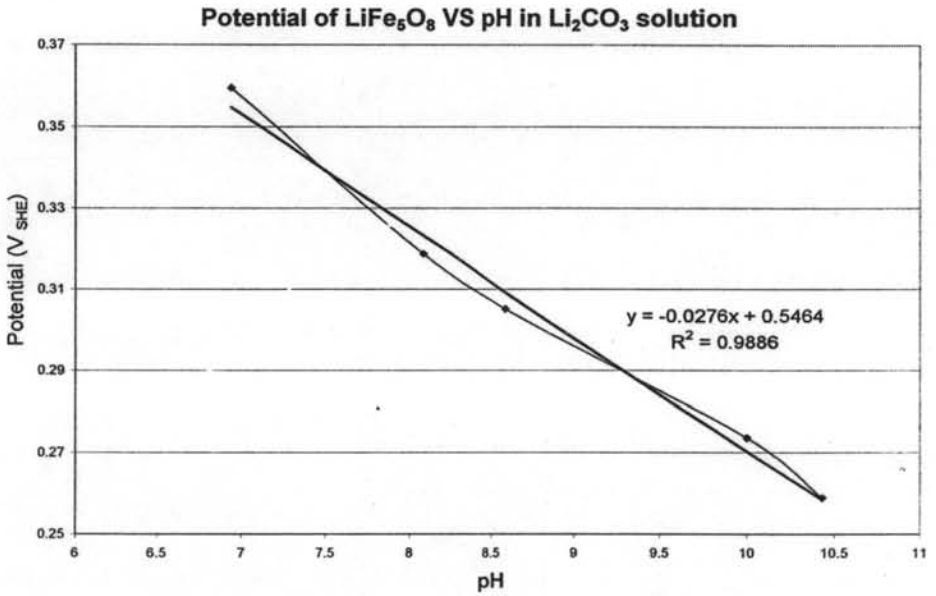

Figure 4.9 Potential vs pH at 10^{-3} M Li_2CO_3 test solution at room temperature.

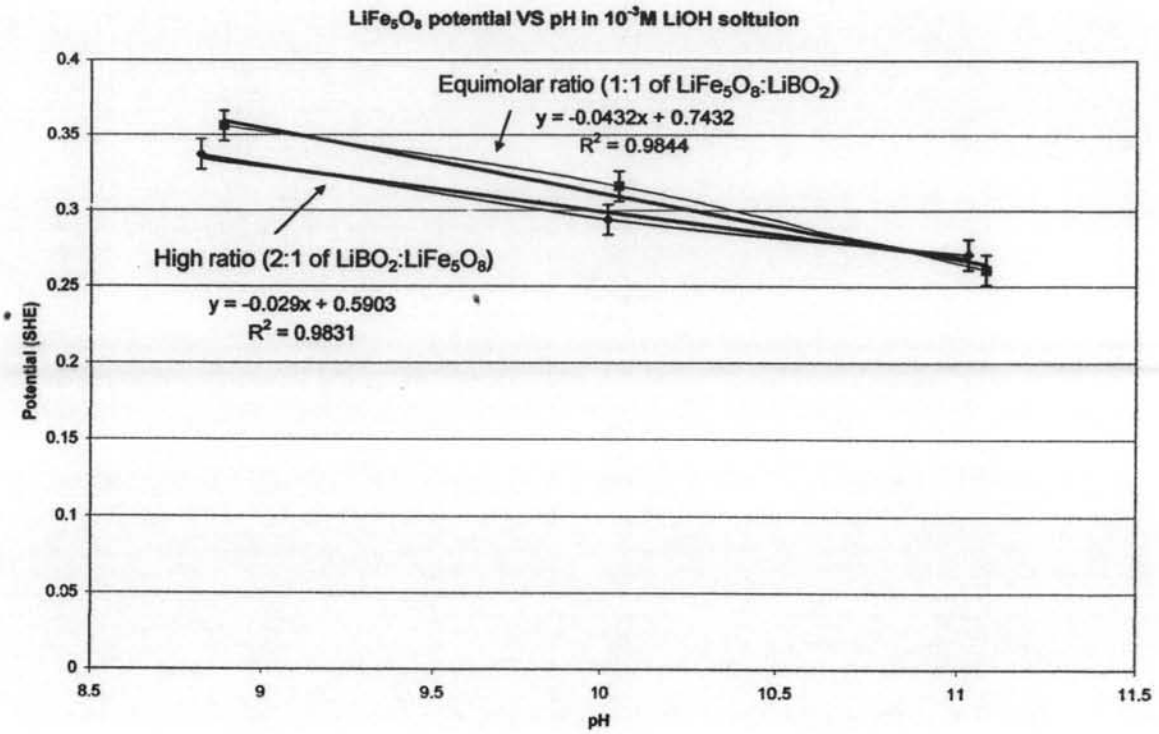

Figure 4.10 Potential vs pH at 10^{-3} M LiOH test solution at room temperature.

4.3 Reaction Hypothesis

It is proposed that the following reaction is occurring,

$$LiFe_5O_8 + e^- + 2H^+ \rightarrow Li^+ + Fe_5O_7 + H_2O \qquad (26)$$

Where Fe_5O_7 is probably not the actual compound formed but fits the stoichiometry and will be examined later.

The Nernst equation will give the following trends, neglecting the activity coefficient:

$$E = E^o - \frac{RT}{nF}\ln\frac{[Li^+]}{[H^+]^2} \qquad (27)$$

$$E = E^o - \frac{2.303RT}{nF}\log[Li^+] + \frac{2\times 2.303RT}{nF}\log[H^+] \qquad (28)$$

$$\because pH = -\log[H^+] \tag{29}$$

$$\therefore E = E^o - \frac{2.303RT}{nF}\log[Li^+] - \frac{2\times 2.303RT}{nF}(pH) \tag{30}$$

$$E = B - m(pH) \tag{31}$$

Where B and m are the intercept and slope of the graph in Figure 4.9.
Equation (28) is valid only when lithium ferrite remains fixed.

The number of electrons can also be determined from the slope of Potential vs pH graph since all the parameters are fixed. Thus, at 25°C,

$$Slope = \frac{0.1183}{n} \tag{32}$$

From Figure 4.9, the number of electrons was calculated to be 4.28 (≈ 4) while Figure 4.10, indicates the number of electrons when the equimolar and high ratio $LiFe_5O_8$ electrode were tested and found to be 2.74 and 4.07 (≈ 4) respectively. This seems contradictory to the proposed reaction (with one electron transfer).

Since the potential is also a function of concentration, Figure 4.11 is a plot between potential versus lithium concentration. This was done by using a solution of lithium hydroxide (LiOH) with lithium chloride (LiCl) to vary the lithium concentration. The number of electrons transferred in the equilibrium can be determined from the slope of this graph by rearranging equation (30) to give:

$$E = A - m\log[Li^+] \tag{33}$$

Where A and m are the intercept and the slope of the graph in Figure 4.11.

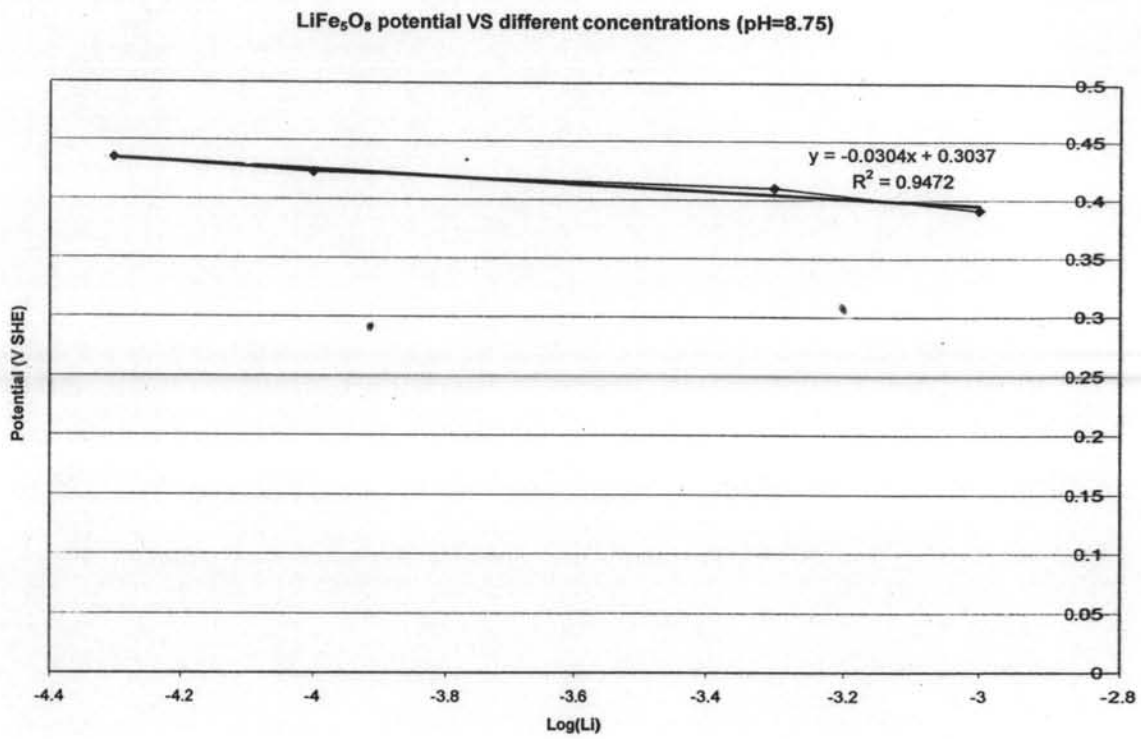

Figure 4.11 Potential versus lithium concentrations in buffer solution (LiOH) with an addition of LiCl.

Once again, the number of electrons transferred in the equilibrium reaction was calculated to be 1.94 (≈ 2) which opposes the proposed reaction.

The summary of potential measurements in solution of different lithium compounds at various concentrations is tabulated in Table 4.2.

Table.4.2 Summary of $LiFe_5O_8$ potential measurements in solution of different lithium compound at various concentrations

Potential measurement (V_{SCE})	Li_2CO_3			LiOH		
	10^{-3}M	10^{-4}M	10^{-5}M	10^{-3}M	10^{-4}M	10^{-5}M
High ratio	70±3mV	127±7mV	54±2mV	28±2mV	52±2mV	95±1mV
Equimolar ratio	65±5mV	128±3mV	88±5mV	18±2mV	78±4mV	110±3mV

From Table 4.2, both the equimolar and high ratio preparation of $LiFe_5O_8$ in Li_2CO_3 solution produced potentials which seem inconsistent with the proposed reaction through the Nernst equation; that is the higher the lithium concentration in

solution, the lower the potential. In LiOH solution, both the equimolar and high ratio prepared ferrite produced more reasonable potentials according to the Nernst equation. Figure 4.12 shows the stability of the measured potential in LiOH solution with different lithium concentrations. For 10^{-4} and 10^{-5} M Li, the potential was established quite quickly whereas with 10^{-3} M Li, it took a much longer time to reach the equilibrium potential of around 30 mV, presumably due to oxide built up on the surface of the electrode.

Figure 4.12 was plotted with primary and secondary X-axes. The 10^{-3}M Li curve belongs to the secondary X-axes, indicated on the top of the graph whereas the others belong to the primary X-axis indicated at the bottom of the graph.

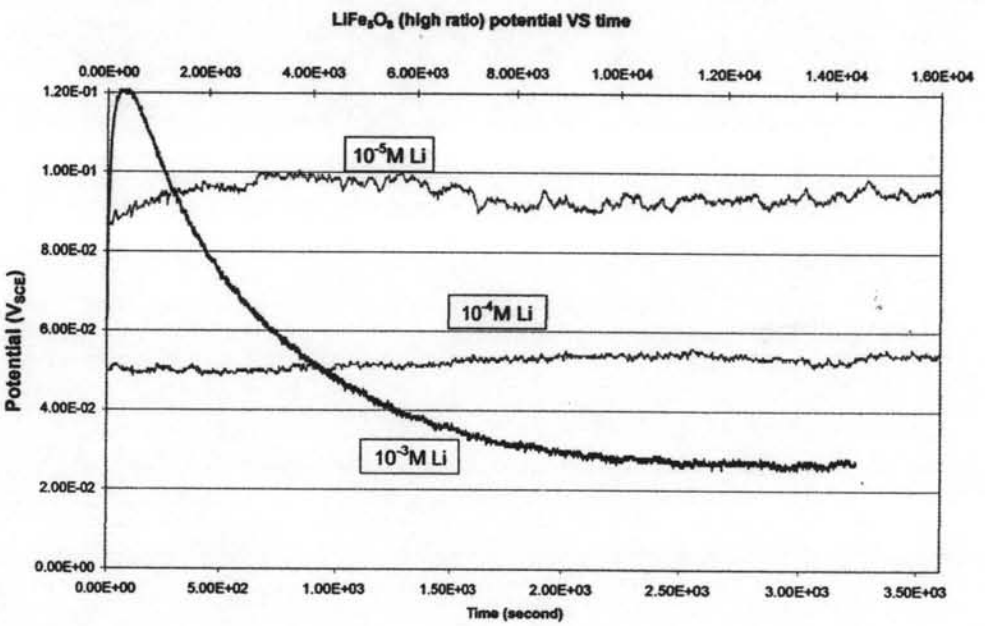

Figure 4.12 Potential stability versus time in LiOH solutions with different Li concentrations.

4.4 Mechanism Validation by Means of The Gibbs Free Energy Calculation

The reaction is proposed to occur as follows;

$$LiFe_5O_8 + e^- + 2H^+ \rightarrow Li^+ + Fe_5O_7 + H_2O \quad (34)$$

The Gibbs free energy of Li^+ and H_2O can be determined from literature values. Kawamura *et al.,* (2001) determined the Gibbs free energy of formation of $LiFe_5O_8$ over the range of temperatures of 673-873K as shown in Figure 4.13.

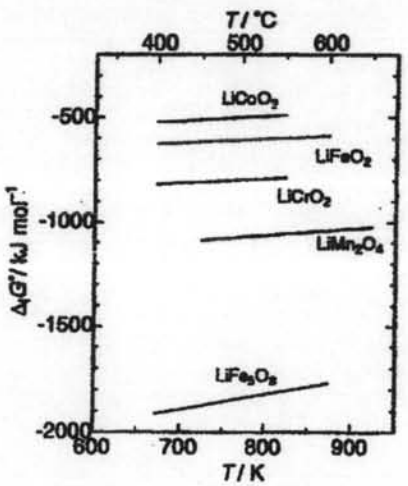

Figure 4.13 The standard Gibbs free energy change of lithium transition metal oxide.

For simplicity, the relationship between the Gibbs free energy of formation and temperature is assumed to be linear and extendable to lower temperatures. Therefore, the Gibbs free energy of formation of $LiFe_5O_8$ at room temperature was determined as -2170.8 kJ/mol.

The Gibbs free energy of reaction is related to the equilibrium potential through;

$$\Delta G^o_{rxn} = -nFE^o \quad (35)$$

The standard potential was determined experimentally from the OCP measurements. In addition, the activity coefficient was included in this calculation for more precise results. After the Gibbs free energy of reaction was determined, the Gibbs free energy of the unknown product (Fe_5O_7) was calculated using the following equation;

$$\Delta G^o_{rxn} = \sum \Delta G^o_{products} - \sum \Delta G^o_{reactants} \tag{36}$$

All calculations are shown in Appendix A.1. The Gibbs free energy of the unknown product (Fe_5O_7) was determined to be -1790±10 kJ/mol in lithium hydroxide solution as shown in Table 4.3 and Table 4.4. By coincidence, the sum of the Gibbs free energy of formation of magnetite and maghemite is around -1745 ± 40 kJ/mol[1], thus it is likely that the product is a combination of γ-Fe_2O_3 and Fe_3O_4 which is consistent with the reaction stoichiometry. After the $LiFe_5O_8$ was tested for several experiments, it was clearly seen that a red compound was formed on the surface of the $LiFe_5O_8$ electrode. This leads to the proposed reaction, written as:

$$LiFe_5O_8 + e^- + 2H^+ \rightarrow Li^+ + Fe_3O_4 + Fe_2O_3 + H_2O \tag{37}$$

Table 4.3 Tabulated values of the Gibbs free energy of Fe_5O_7 from high ratio prepared $LiFe_5O_8$

concentration (M)	pH	E_{SCE}	E_{SHE}	E^o(SHE) (with activity coefficient)	ΔG^o_{rxn} (kJ/mol)	G^o_{Fe5O7} (kJ/mol)
10^{-3}	11.05	0.026	0.267	0.83152887	-160.49	-1800.09
10^{-4}	10.02	0.05	0.291	0.79460437	-153.36	-1792.96
10^{-5}	8.90	0.094	0.335	0.77235637	-149.06	-1788.67

[1] 2000 by CRC Press LLC

Table 4.4 Tabulated values of the Gibbs free energy of Fe_5O_7 from equimolar ratio prepared $LiFe_5O_8$

concentration (M)	pH	E_{SCE}	E_{SHE}	E°(SHE) (with activity coefficient)	ΔG°_{rxn} (kJ/mol)	G°_{Fe5O7} (kJ/mol)
10^{-3}	11.00	0.017	0.258	0.81957137	-158.18	-1797.78
10^{-4}	10.06	0.072	0.313	0.81897037	-158.06	-1797.67
10^{-5}	8.97	0.112	0.353	0.79449687	-153.34	-1792.94

As a further validation, the XRD pattern of the sample scraped from the electrode after the polarization experiment confirmed the presence of maghemite. Figure 4.14 shows the pattern of the sample scraped from the electrode after the experiments. The arrows indicate the position of maghemite peaks which match with the XRD peaks.

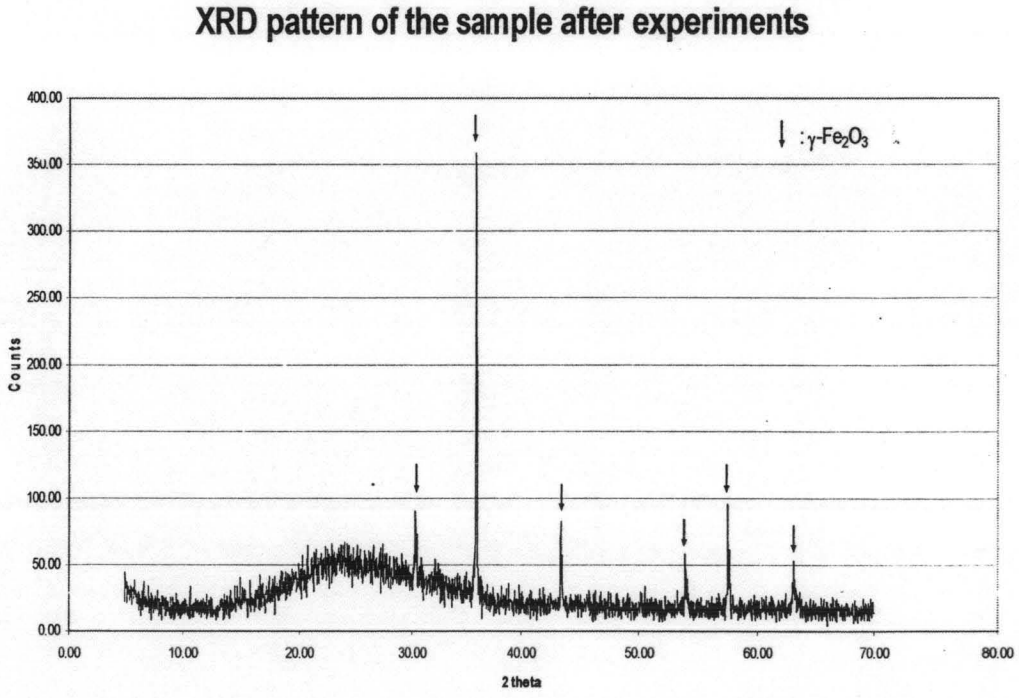

Figure 4.14 XRD pattern of the scrapped sample from $LiFe_5O_8$ after polarization experiments.

4.5 Cyclic Voltammetry (CV)

This electroanalytical measurement is used to determine the mechanism of electrochemical reactions which are taking place, on an electrode. In this study, cyclic voltammetry was used to investigate the validity of the proposed electrochemical reaction of $LiFe_5O_8$. Based on the previous results, the proposed reaction is,

$$LiFe_5O_8 + e^- + 2H^+ \rightarrow Li^+ + Fe_3O_4 + Fe_2O_3 + H_2O \quad (38)$$

This technique was conducted to verify whether the above reaction is equilibrium reaction. The tests were run in solution of different Li_2CO_3 concentrations (10^{-3}M, 10^{-4}M and 10^{-5}M) and the $LiFe_5O_8$ potential was measured until steady potential was achieved before applying CV. This pre-potential measurement ensures a more precise cyclic voltammetry plot. The potential was measured continuously after the CV had been completed for a cycle to ensure it comes back to its original value. A cyclic voltammetry plot in Li_2CO_3 solution is shown in Figure 4.15.

Theoretically, a peak current should be apparent on both forward (positive direction) and reverse (negative direction) scans at a particular potential. From Figure 4.15, it was seen that there is one small peak which occurred at around 450 mV. On the reverse scan, there were several small peaks present which may represent either that multiple reactions of lithium ferrite are occurring or an instability of the three electrode system. The potential difference between the reduction and oxidation peaks is theoretically 59mV for a reversible reaction with one electron transfer. Practically, the difference is typically between 70-100 mV. Larger differences or non symmetric reduction and oxidation peaks are an indication of a non reversible reaction or a system in which a mixed potential has been established. Figure 4.15 indicates that the potential established on the $LiFe_5O_8$ electrode is probably a mixed potential and may possibly be irreversible.

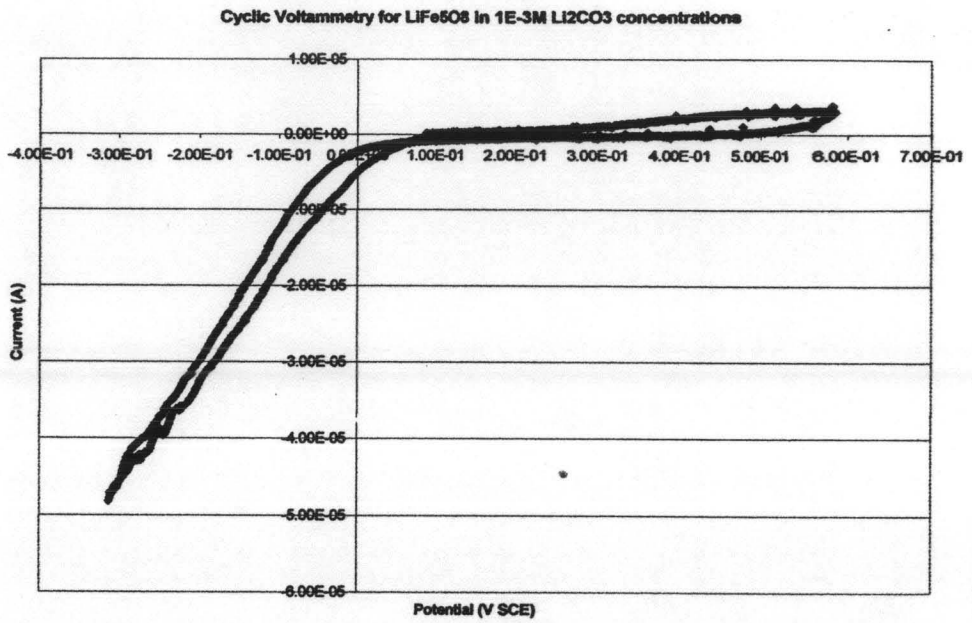

Figure 4.15 Cyclic voltammetry curve of $LiFe_5O_8$ electrode in 10^{-3}M Li_2CO_3 at 1 mV/s scan rate.

Lithium hydroxide was also used as a testing solution. The concentration was varied over the same values as used in the lithium carbonate solutions. The cyclic voltammetry in 10^{-3}M LiOH solution is shown in Figure 4.16 to verify the proposed reaction.

From Figure 4.16, it is shown that the potential established is most probably a mixed potential since two peaks were seen quite far from the equilibrium potential. The peak potential and current were determined as -0.577 V_{SCE} and-1.32 x 10^{-4} A respectively. Hence, the half peak potential and current were calculated. By applying the characteristic equations of cyclic voltammetry, the number of electrons in this reaction was approximately equal to 2. The calculation is shown in Appendix A.2.

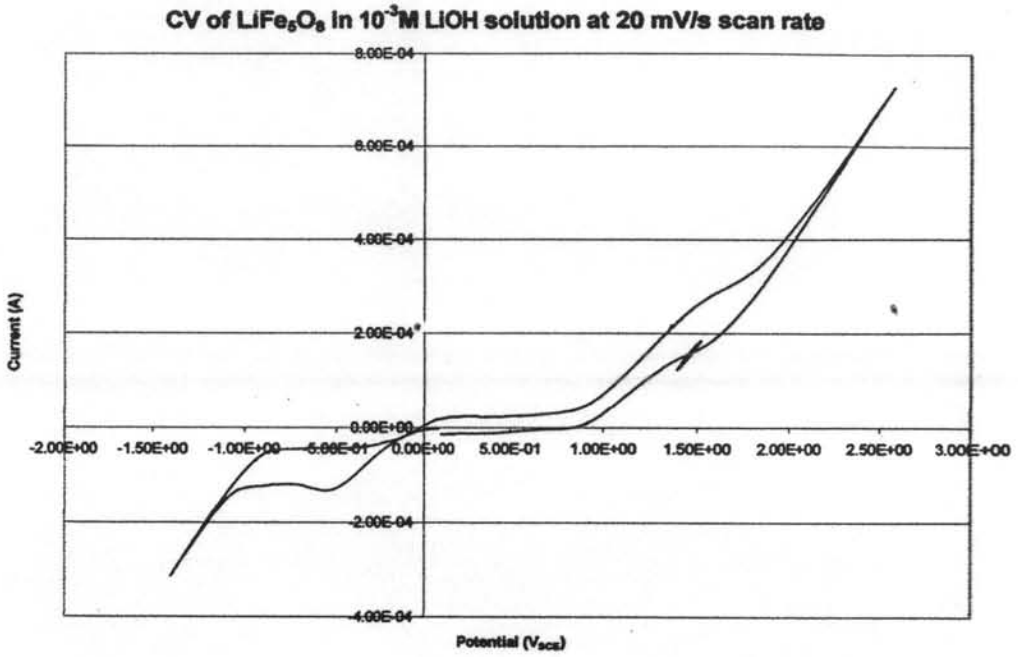

Figure 4.16 A cyclic voltammetry in 10^{-3}M LiOH solution at 20 mV/s scan rate.

Cyclic voltammetry was performed in the buffer solution as shown in Figure 4.17. The test solution in this system is the NH_4Cl buffer solution used previously with the addition of LiCl to vary lithium concentration. The 10^{-4} M Li was chosen as this test solution. Figure 4.17 shows what appears to be quasi-reversible behavior of $LiFe_5O_8$ in the buffer solution. At a scan rate of 1mV/s, both cathodic and anodic peaks seem to be symmetrical relative to one another which indicates a reversible system. However, at a higher scan rate (10 mV/s), the cathodic current peaks were established at much higher values than the anodic current peaks, indicating an irreversible system. It can be pointed out that a different equilibrium reaction probably is taking place in the buffer solution than occurred in either Li_2CO_3 or LiOH solutions. From the 1 mV/s scan rate, it was almost certain to be a reversible reaction because the ratio of the anodic peak current to the cathodic peak current is almost equal to one (for reversible process, $\left|\frac{i_{pa}}{i_{pc}}\right| = 1$). For both 1 mV/s and 10 mV/s scan rate, the potential separation between cathodic and anodic peaks was 130 mV

and 280 mV respectively. This set of information possibly indicates the quasi-reversible behavior.

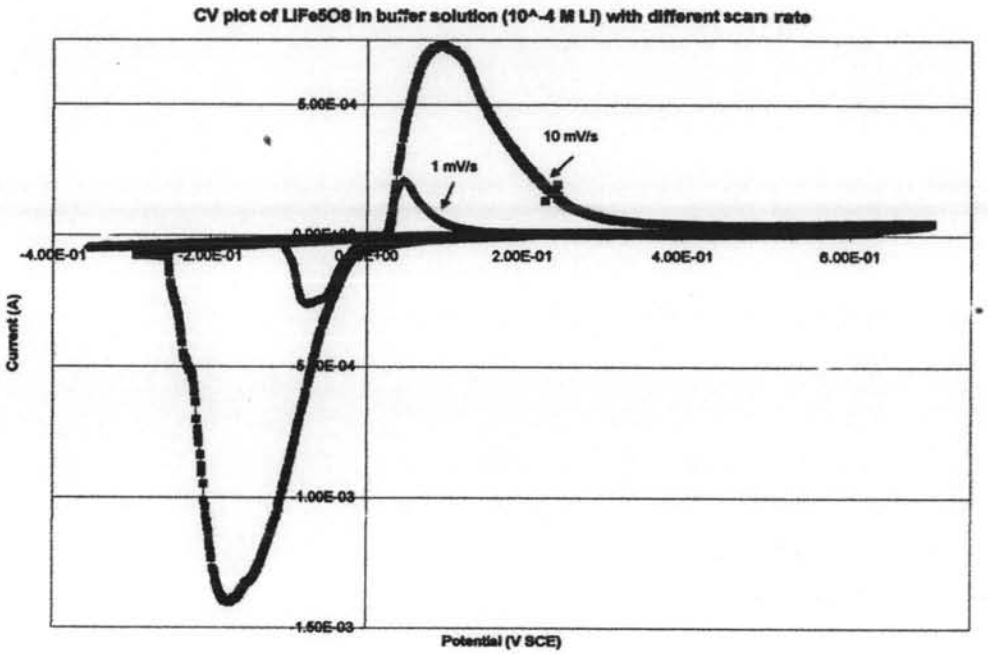

Figure 4.17 Cyclic voltammetry of $LiFe_5O_8$ in buffer solution at 10^{-4} M lithium with different scan rates.

4.6 High Temperature Measurements

The high temperature measurement was conducted with the three electrode system in a titanium autoclave. This system contains the working electrode (WE), reference electrode (RE) and counter electrode (CE) as before. A palladium wire coated with lithium ferrite was used as the working electrode and a platinum wire was used as the reference electrode to establish reversible hydrogen potential. However, the reversible hydrogen potential can be achieved only in hydrogenated solutions. Therefore hydrogen was purged into the system until the system became saturated. Another reason for hydrogen purging is to eliminate the oxygen in the system. A carbon steel coupon was used as counter electrode which acts as a current carrier to the system.

The $LiFe_5O_8$ was tested to determine its stability in high temperature and high pressure conditions in the autoclave. Initially, hydrogen was purged into the system until saturation, thus a standard hydrogen potential was established. The OCP and CV were measured alternately as the temperature was increased from 25°C to 300°C in increments of 50°C. For each increment, a potential achieved a stable value. Figure 4.18 shows the potential measurements of $LiFe_5O_8$ in the autoclave as the temperature was increased. The overall behavior of $LiFe_5O_8$ electrode in the autoclave as temperature was increased is as indicated by the Nernst equation; potential is inversely proportional to temperature. Each declining potential indicated the time interval when the temperature was raised while each plateau indicates the establishment of the potential at that particular temperature. After the $LiFe_5O_8$ was tested at high temperature for two high temperature runs, more than half of the original quantity was lost or decomposed. This possibly indicates the instability of $LiFe_5O_8$ under high temperatures and pressures.

This result from this test is invalided at above 200°C due to a leak from one of the fittings on the autoclave. This leads to improper behavior of the potential from 200°C onward, which opposes to the Nernst equation. Especially, at 300°C, a huge noise was presented after it had been left overnight. Nevertheless, it is evident that $LiFe_5O_8$ can not withstand such severe conditions as it decomposed during the autoclave test. The cyclic voltammetry technique was also performed to check the validity of the $LiFe_5O_8$ electrode shown in Figure 4.19. It seems that no electrode reaction occurred on the electrode in the autoclave during the high temperature experiment. The fluctuation in the positive potential and current region indicates a temperature fluctuation from the temperature controller. However, no reaction was shown during the time interval.

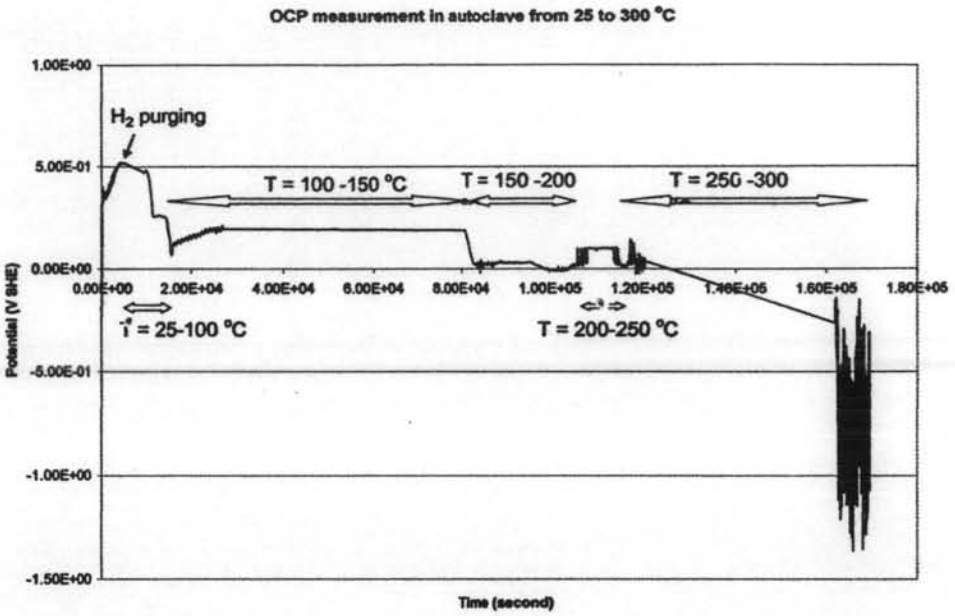

Figure 4.18 $LiFe_5O_8$ potential measurement under high temperature and pressure in the autoclave up to 200°C.

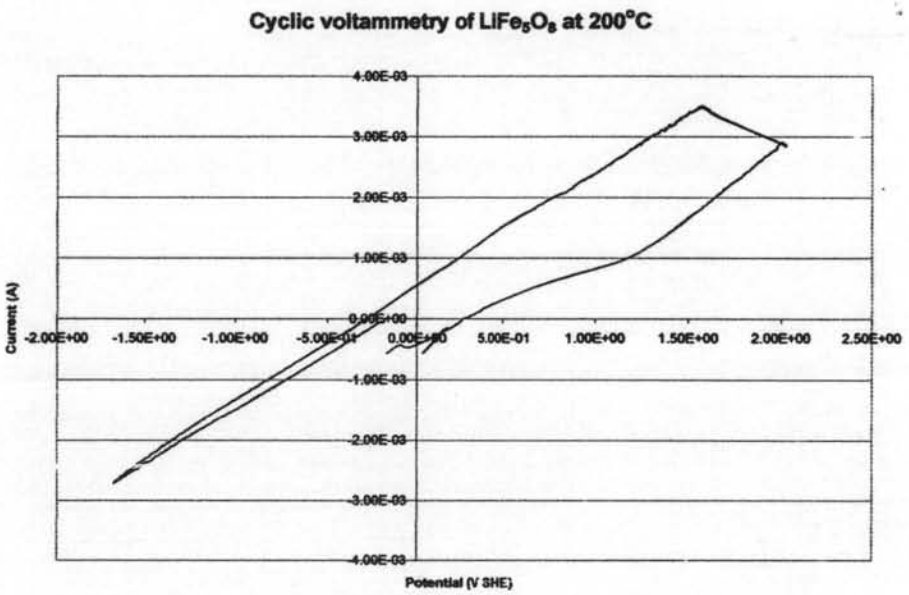

Figure 4.19 Cyclic voltammetry of $LiFe_5O_8$ at 200°C in the autoclave.